Songklanakarin J. Sci. Technol.
47 (6), 388–395, Nov. – Dec. 2025

http://www.sjst.psu.ac.th

Original Article

3D-QSAR studies of 4-aminoquinoline-pyrimidine hybrids as antimalarial inhibitors targeting wild-type *P. falciparum* dihydrofolate reductase

Jitrayut Jitonnom[1, 2*], Wijitra Jitonnom[1, 2], Panthip Tue-ngeun[1, 3], Patchreenart Saparpakorn[4], Supa Hannongbua[4], and Warot Chotpatiwetchkul[5*]

[1] *Unit of Excellence in Computational Molecular Science and Catalysis, University of Phayao, Mueang, Phayao, 56000 Thailand*

[2] *Division of Chemistry, School of Science, University of Phayao, Mueang, Phayao, 56000 Thailand*

[3] *Program in Chemistry, Faculty of Science and Technology, Uttaradit Rajabhat University, Mueang, Uttaradit, 53000 Thailand*

[4] *Department of Chemistry, Faculty of Science, Kasetsart University, Chatuchak, Bangkok, 10900 Thailand*

[5] *Applied Computational Chemistry Research Unit, Department of Chemistry, School of Science, King Mongkut's Institute of Technology Ladkrabang, Lat Krabang, Bangkok, 10520 Thailand*

Received: 27 November 2024; Revised: 27 May 2025; Accepted: 13 August 2025

Abstract

Three-dimensional quantitative structure–activity relationship (3D-QSAR) was determined on a set of 4-aminoquinoline-pyrimidine hybrids to elucidate the 3D structural features affecting the antimalaria activity against wild-type *Plasmodium falciparum* dihydrofolate reductase (*Pf*DHFR). Several combined analyses of comparative molecular field (CoMFA), comparative molecular similarity indices (CoMSIA) and noncovalent interaction (NCI) were carried out. The 3D descriptors capturing steric, electrostatic and hydrophobic features of molecules and their correlation with experimental activity were established (CoMFA; $q^2 = 0.506$, $r^2 = 0.875$, SEE = 0.227 and CoMSIA; $q^2 = 0.614$, $r^2 = 0.871$, SEE = 0.230). Key structural features are drawn from the models: The R^1 substituent prefers small, less steric groups, while the R^2 substituent favors larger, more sterically bulky hydrophobic groups. Introducing hydrogen bond acceptor and donor groups at R^2 and the N-substituted linkage enhances activity. The docking and NCI results revealed extensive hydrophobic interactions and its stabilization to the binding process of *Pf*DHFR.

Keywords: Malaria, QSAR, molecular docking, aminoquinoline-pyrimidine, CoMFA, CoMSIA

*Corresponding author
Email address: jitrayut.ji@up.ac.th, warot.ch@kmitl.ac.th

1. Introduction

Malaria is caused by any of five species of Plasmodium, with *P. falciparum* being the most dangerous (Phillips *et al*., 2017). It is spread to people by the bite of a female Anopheles mosquito. The 2023 WHO Report links climate change to malaria via effects on mosquito behavior and survival (Venkatesan, 2024). Global malaria cases rose to 249 million in 2022, exceeding pre-pandemic levels. Climate change impacts, such as drug and insecticide resistance, humanitarian crises, and resource constraints, pose significant risks to progress against malaria, particularly in vulnerable regions. In Pakistan, 2022 flooding led to a fivefold rise in malaria cases.

Dihydrofolate reductase from *Plasmodium falciparum* (*Pf*DHFR) is a key antimalarial target, but resistance has reduced the efficacy of current drugs (Chakraborty, 2016; Gelb, 2007; Sharma & Chauhan, 2012). Thus, new, potent antimalarials are urgently needed. Hybrid molecules, which combine pharmacophores to act on multiple targets, are a promising approach to overcoming resistance, including in treatment of malaria (Muregi & Ishih, 2010). Various 4-aminoquinoline and pyrimidine-based hybrids have shown promising activity against sensitive and resistant *P. falciparum* strains. Yuthavong *et al*. (Tarnchompoo *et al*., 2002) first introduced 2,4-diaminopyrimidines for antimalarial activities against PfDHFR (Figure 1A, B). Manohar *et al*. reported 4-aminoquinoline-triazine conjugates with antimalarial efficacy against chloroquine-sensitive and resistant *P. falciparum* strains (Figure 1C) (Manohar, Khan, & Rawat, 2010). Balabadra *et al*. evaluated a novel family of naphthyl-bearing 1,2,3-triazoles for in vitro antiplasmodial activity against pyrimethamine (Pyr)-sensitive and Pyr-resistant *P. falciparum* strains (Figure 1D) (Balabadra *et al*., 2017). Novel 4-aminoquinoline-purine hybrids were also reported with antiplasmodial against chloroquine-sensitive and chloroquine-resistant *P. falciparum* strains (Figure 1E) (Reddy, Khan, Ponnan, Tripathi, & Rawat, 2017). Novel triazine–pyrimidine compounds (Figure 1F) were produced and tested for *in vitro* antimalarial activity in 2014 (Kumar, Khan, Ponnan, & Rawat, 2014). All compounds showed higher activity (IC_{50} = 1.32–10.70 μM) than the pyrimethamine (>19 μM) against the chloroquine-resistant strain W2. Rawat's group has reported numerous 4-aminoquinoline-pyrimidine hybrids (Figure 1G) with strong antimalarial activity (Kumar, Khan, Tekwani, Ponnan, & Rawat, 2014, 2015; Manohar *et al*., 2015; Manohar, Rajesh, Khan, Tekwani, & Rawat, 2012; Manohar, Tripathi, & Rawat, 2014; Maurya, Khan, Bahuguna, Kumar, & Rawat, 2017; Tripathi, Khan, Ponnan, Kholiya, & Rawat, 2017; Thakur, Khan, & Rawat, 2014; Tripathi, Khan, Thakur, Ponnan, & Rawat, 2015).

Three-dimensional quantitative structure−activity relationship (3D-QSAR) is a ligand-based drug design approach that has significantly advanced drug discovery (Roy, Kar, & Das, 2015). Among the well-established 3D-QSAR techniques, comparative molecular field analysis (CoMFA) (Cramer, Patterson, & Bunce, 1988) and comparative molecular similarity indices analysis (CoMSIA) (Klebe, Abraham, & Mietzner, 1994) provide valuable guidance for designing potent ligands by identifying 'favorable' or 'unfavorable' regions around the molecules through contour map visualization. In this study, CoMFA and CoMSIA were employed to construct 3D-QSAR models capturing the pharmacophoric features of 4-aminoquinoline-pyrimidine compounds based on their 3D structures and antimalarial inhibitory activities (IC_{50}). Molecular docking (Jones, Willett, Glen, Leach, & Taylor, 1997; Tue-ngeun *et al*., 2024) was used to predict the binding poses and interactions of each compound, using the X-ray structure of *Pf*DHFR bound with pyrimethamine (PDB ID: 3QGT) as a template (Figure 2). Additionally, noncovalent interaction (NCI) analysis further characterized the binding interactions, providing insights into the structural requirements for antimalarial activity.

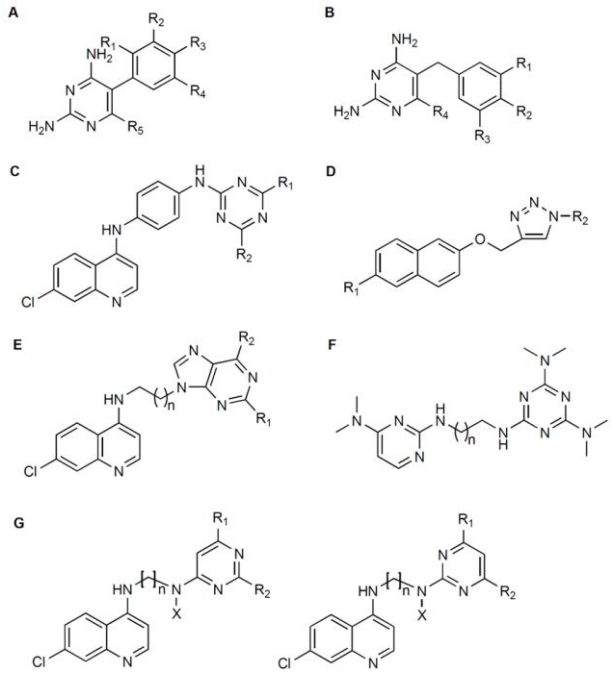

Figure 1. Structures of 4-aminoquinoline-based and pyrimidine-based compounds with antimalarial inhibitory activity against *Pf*DHFR included in Table S1. 4-aminoquinoline-pyrimidine compounds used in the current 3D-QSAR study are indicated in panel G.

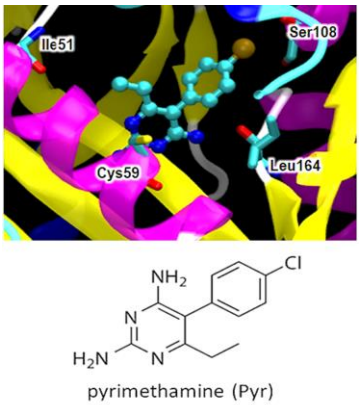

Figure 2. Structures of wild-type *Pf*DHFR when complexed with an antimalarial drug, pyrimethamine (Pyr), that was used in this current 3D-QSAR study. Coordinates were taken from PDB ID 3QGT.

2. Materials and Methods

2.1 Data set

A total of 162 compounds of 4-aminoquinoline-pyrimidine derivatives with reported IC_{50} values were compiled from previous studies (Kumar, Khan, Ponnan, & Rawat, 2014; Kumar, Khan, Tekwani, Ponnan, & Rawat, 2015; Manohar, Rajesh, Khan, Tekwani, & Rawat, 2012; Maurya, Khan, Bahuguna, Kumar, & Rawat, 2017; Tripathi, Khan, Ponnan, Kholiya, & Rawat, 2017; Tripathi, Khan, Thakur, Ponnan, & Rawat, 2015). The Sybyl-X 2.0 program (Tripos, USA) was used for 3D-QSAR modeling. Compounds were divided into a training set (130 compounds) and a test set (32 compounds), selected to ensure diversity in biological activity and structure. The dataset was selected on the basis of linker length (*n*), N-substituents (–NX), and pyrimidine ring substituents (R_1, R_2). The IC_{50} and pIC_{50} values ($pIC_{50} = -\log IC_{50}$) as well as compound structures can be found in Table S1.

2.2 Molecular docking

All compounds were built in Discovery Studio (BIOVIA, 2017) and geometry-optimized at the M06-2X/6-31G(d) level using Gaussian 09 Revision D.01 (Frisch *et al*., 2009). Gasteiger-Hückel charges were assigned to the compounds. Docking was performed using GOLD (Verdonk, Cole, Hartshorn, Murray, & Taylor, 2003) with the *Pf*DHFR crystal structure (PDB ID: 3QGT, chain A) as receptor (Vanichtanankul *et al*., 2011). The cofactor NADPH (hereafter referred to as NDP) was retained; water and pyrimethamine were removed. Hydrogen atoms were added, and residues within 12 Å of the binding site were defined as the docking region. A genetic algorithm was applied to explore ligand poses, performing 100 docking runs per compound. GoldScore was used to rank the binding poses. The protocol was validated by re-docking the co-crystal ligand (RMSD < 1.0 Å). The highest-scoring pose of compound 57 served as the alignment template for QSAR analysis.

2.3 CoMFA and CoMSIA analyses

QSAR models were developed in Sybyl-X using the docked conformations. CoMFA used Lennard–Jones and Coulomb potentials; CoMSIA included five fields: steric, electrostatic, hydrophobic, H-bond donor, and acceptor. A 2.0 Å grid and a distance-dependent dielectric were applied. A Gaussian-type, distance-dependent function was used to calculate molecule properties. The leave-one-out (LOO)

Table 1. Actual and predicted pIC_{50} activities (denoted as Act pIC50 and Pred pIC50, respectively) for the test set (32 compounds) of CoMFA and CoMSIA. The difference in their residual activity (Δ) is also included. Full IC_{50} and pIC_{50} values can be found in Table S1.

Compound	n(linker)	R_1	R_2	Act pIC_{50}	CoMFA model		CoMSIA model	
					Pred pIC50	Δ	Pred pIC50	Δ
9	3	NH-4-F,Ph	H	7.553	7.231	-0.382	7.255	-0.298
10	3	NH-4-Cl,Ph	H	7.328	7.363	-0.072	7.275	-0.053
11	3	NH-4-Br,Ph	H	7.31	7.210	-0.149	7.235	-0.075
12	3	NH-4-CH_3,Ph	H	6.815	7.242	0.405	7.298	0.483
15	4	NH-Ph	H	7.357	6.984	-0.541	7.179	-0.177
25	2	NH-4-Br,Ph	Methyl	7.252	7.487	-0.043	7.323	0.071
30	3	NH-4-F,Ph	Methyl	7.237	7.116	-0.222	7.305	0.068
31	3	NH-4-Cl,Ph	Methyl	7.222	7.093	-0.190	7.279	0.057
44	3	Methyl	Chloro	6.481	6.356	-0.031	7.208	0.726
45	4	Methyl	Chloro	6.921	6.827	-0.179	7.302	0.381
48	3	Methyl	Chloro	6.62	6.535	-0.065	7.083	0.463
50	6	Methyl	Chloro	6.854	7.496	0.429	7.494	0.640
62	4	Methyl	*N*-Et piperazine	7.699	7.639	0.070	7.578	-0.121
71	3	H	NH-$(CH_2)_5$OH	5.412	5.484	0.129	5.632	0.220
76	3	Methyl	NH-$(CH_2)_5$OH	5.578	5.983	0.465	5.947	0.369
81	4	H	NH-$(CH_2)_6$OH	5.499	6.068	0.604	6.146	0.647
84	4	Methyl	NH-$(CH_2)_4$OH	6.886	6.211	-0.650	5.948	-0.938
87	2	Methyl	Chloro	7.194	6.677	-0.535	6.967	-0.227
102	2	Methyl	*N*-Et piperazine	7.377	7.342	0.031	7.255	-0.122
103	2	Methyl	Pyrrolidine	7.222	7.607	-0.164	7.034	-0.188
104	2	Methyl	Piperidine	7.357	7.343	0.017	7.086	-0.271
109	3	Methyl	Morpholine	7.276	7.408	0.036	7.170	-0.105
112	3	Methyl	Chloro	5.955	6.721	0.744	6.620	0.665
118	2	Methyl	4-Ethylpiperazin-1-yl	7.699	7.435	-0.178	7.463	-0.236
122	3	Methyl	4-Ethylpiperazin-1-yl	7.398	7.388	-0.084	7.329	-0.069
126	2	Methyl	4-Ethylpiperazin-1-yl	7.523	7.191	-0.330	7.108	-0.415
129	3	Methyl	Morpholin-1-yl	6.886	6.936	0.042	6.540	-0.346
136	3	Methyl	Piperidin-1-yl	7.292	7.314	0.080	7.178	-0.115
139	3	H	Pyrrolidin-1-yl	6.690	6.745	-0.001	6.908	0.217
153	4	H	Morpholin-1-yl	7.420	7.266	-0.159	7.196	-0.224
159	6	Methyl	Pyrrolidin-1-yl	7.102	7.177	-0.032	7.409	0.307
160	6	Methyl	Piperidin-1-yl	7.092	7.161	-0.037	7.419	0.327

cross-validation (q^2) was used to assess the performance of the models. The predictive ability within the test set (32 compounds) was obtained using the equation r^2_{pred}= (SD-PRESS)/SD, where SD is the sum of squared deviations between the mean activity of the training set and the inhibitory activities of the test set. PRESS is the sum of squared deviations between the predicted and experimental activity for each compound in the test set. Molecular visualization was generated using Discovery Studio and Sybyl-X.

2.4 Noncovalent interaction

NCI analysis of the most active compounds (57–59) was performed via the NCIweb server (https://nciweb.dsi.upmc.fr/) (Novoa, Laplaza, Peccati, Fuster, & Contreras-García, 2023). The method analyzes weak interactions through electron density (ρ) and reduced density gradient (s, also referred to as RDG) using promolecular densities (Contreras-García *et al*., 2011). 3D isosurfaces (cutoff = 0.3 a.u.) reveal hydrogen bonds (blue), van der Waals (green), and repulsive (red) interactions.

3. Results and Discussion

3.1 General information on the compounds

A set of 4-aminoquinoline-pyrimidine derivatives with a broad pIC_{50} range (4.980–8.301) was investigated using 3D-QSAR modeling. Actual and predicted pIC_{50} values for the 32 test set compounds are shown in Table 1; data for the remaining compounds appear in Table S1. Test compounds were randomly selected to reflect both structural diversity and biological activity. Differences in inhibitory activity against the chloroquine-sensitive *P. falciparum* D6 strain were attributed to structural variations (Table 1). The distribution of compounds with different linker lengths (n = 2, 3, 4, and 6) is summarized in Figure 3. The most common linker length was n = 3 (39%), followed by n = 2 (30%) and n = 4 (25%), as shown in the pie chart (Figure 3B). No compounds with n = 5 were found, and only 6% had the longest linker (n = 6). These trends suggest that an optimal alkyl linker length contributes to the antimalarial activity.

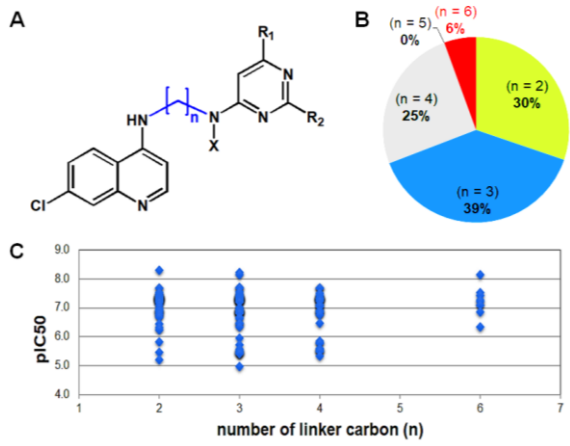

Figure 3. Population of compounds with different numbers of linker carbons (*n*), as observed from the 162 compounds with antimalarial activities (pIC_{50}).

3.2 3D-QSAR

To explore the structure–activity relationship of 162 aminoquinoline-pyrimidine derivatives (Table S1), we applied CoMFA and CoMSIA using the Partial Least Squares (PLS) method (Wold, Ruhe, Wold, & Dunn, 1984). Structures were generated in Discovery Studio 2017 using compound 57 as a template, and geometry-optimized with Gaussian 09. Ten models for each technique were developed, with Model 10 providing the best statistical performance with the highest r^2 (Tables S2–S3). For CoMFA, the optimal model (NOC = 6) had q^2 = 0.506, r^2 = 0.875, F = 133.007, and SEE = 0.227, with steric and electrostatic contributions of 59.8% and 40.2%, respectively (Table 2). CoMSIA, using five descriptors—steric (S), electrostatic (E), hydrophobic (H), H-bond donor (D), and H-bond acceptor (A)—gave q^2 = 0.614, r^2 = 0.871, and the following contributions: A (24.2%) > D (22.1%) > H (19.9%) > E (18.5%) > S (15.3%).

To assess the reliability of the CoMFA and CoMSIA models, both models were trained on the same dataset (Table S1) and validated with a test set of 32 compounds, chosen for structural and activity diversity. Table 1 summarizes predicted and actual activities, and residuals, for the test set. The test set predictions showed good agreement with experimental values ($\Delta < 0.9$). Cross-validation ($q^2 > 0.6$) further supports the predictive reliability of both models.

Contour maps were generated to interpret CoMFA and CoMSIA results using compound 57 (pIC_{50} = 8.301) as reference. CoMFA steric maps (Figure 4A) highlight favorable bulk at R_2 (green contours) and minimal substitution at R_1. Compounds 43, 65, and 57 with increasing steric bulk at R_2 (Cl < $NH(CH_2)_4OH$ < N-methylpiperazine) show increased pIC_{50} values (Figure S1). Similar trends were found for the n = 3 linker series: compound activity followed the order piperidine < morpholine < N-methylpiperazine < N-ethylpiperazine (compounds 51, 55, 58, and 61; Figure S2). For longer linkers (n = 4), steric hindrance near the pyrimidine ring (yellow contours) reduced activity (compounds 15, 36, 45, 52; Figure S3–S4). CoMFA electrostatic maps (Figure 4B) show favorable blue contours at R_2 (positive electrostatics) and red at R_1 (negative). Compounds with electron-donating R_2 groups (e.g., H, Me) showed higher pIC_{50} values than those with electron-withdrawing groups (e.g., Cl, $NH(CH_2)_3OH$), as seen in compounds 18, 39, 45, and 83 (Figure S5–S6).

CoMSIA hydrophobic fields (Figure 5A) show favorable hydrophobicity (purple contours) at R^2. Polar ring systems at R^2—e.g., N-methylpiperazine in compound 57—enhance activity, while hydrophobicity on the pyrimidine ring and linker is disfavored (green contours), as confirmed by compounds 45 and 59 (n = 4; Figure S8–S9) and contrasted with n = 3 compounds (51, 61, 75). H-bond donor fields (Figure 5B) reveal cyan contours near NH linkers and quinoline moieties, suggesting their positive impact. H-bond acceptor fields (Figure 5C) show magenta contours around nitrogen atoms in N-methylpiperazine, consistent with high pIC50 in compounds 57–59 (Figure S10). These observations align with CoMSIA descriptor contributions (Table 2), where H-bond donor and acceptor fields are the most dominant (>40%).

Table 2. Comparison of PLS fitting results between the best CoMFA and CoMSIA models

Model	Leave one out cross-validation		Non-cross-validation			Field contribution (%)				
	q^2	NOC	r^2	SEE	F	S	E	H	D	A
CoMFA	0.506	6	0.875	0.227	133.007	59.8	40.2	-	-	-
CoMSIA	0.614	6	0.871	0.230	128.652	15.3	18.5	19.9	22.1	24.2

q^2; LOO cross-validated correlation coefficient, NOC; the optimum number of components, r^2; non-cross-validated correlation coefficient, SEE; standard error estimate of non-cross-validated correlation coefficient, F; Fisher's values, S; steric, E; electrostatic, H; hydrophobic, D; hydrogen bond donor, A; hydrogen bond acceptor

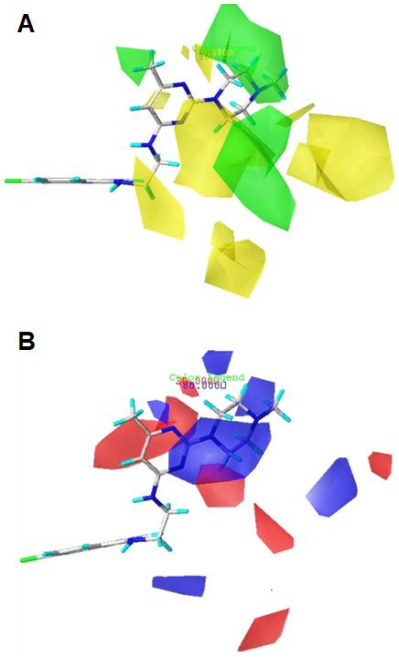

Figure 4. CoMFA contour maps of (A) steric and (B) electrostatic fields using compound 57 as a reference. Green (80%) and yellow (20%) contours in *panel A*, and blue (80%) and red (20%) contours in *panel B* indicate favorable and unfavorable regions, respectively.

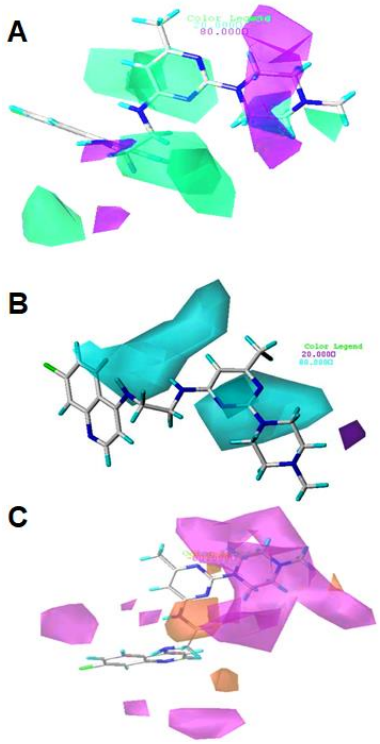

Figure 5. CoMSIA contour maps of (A) hydrophobic, (B) H-bond donor, and (C) H-bond acceptor fields using compound 57 as reference. Favorable and unfavorable regions are shown as: (A) purple (80%) and green (20%), (B) cyan (80%) and purple (20%), and (C) magenta (80%) and orange (20%), respectively.

3.3 Docking simulation

Molecular docking is an *in-silico* method that enables prediction of ligand binding poses and affinities at protein active sites, making it essential in pharmaceutical research (Jitonnom *et al*., 2024; Tue-ngeun *et al*., 2024). In this study, the GOLD program was used to evaluate the binding of 4-aminoquinoline-pyrimidine inhibitors at the *Pf*DHFR active site, offering structural insights for compound design.

Compounds 57–59, among the most active derivatives (pIC_{50} = 7.699–8.301), were selected to represent binding interactions (Figures 6 and S12). All three exhibited both electrostatic and hydrophobic interactions with *Pf*DHFR. Compound 57 formed C–H bonds with Ile14 and Ile164, π–π stacking with Phe58, π–alkyl interactions with Leu46 and Ile112, and a halogen bond (–NH···Cl, 2.8 Å) with Met55. Additional hydrogen bonds with pyrimidine and chloroquine moieties were observed (~2.2 and ~2.6 Å; Figure S12(A)).

Compounds 58–59, with longer linkers, formed more hydrogen bonds (Asp54, Ser111, Ile164, NDP) and hydrophobic interactions (Ala16, Met55, Phe58, Met104, Ile112) (Figures 6C, 6D, S12(B–C)). Unlike 57, where the N-methylpiperazine oriented toward Phe116, compounds 58–59 repositioned the chloroquine moiety to interact with Phe116 and Met55, while the R_2 group stacked with Phe58. Both formed additional π and hydrogen bond contacts with the nicotinamide and ribose moieties of NDP, absent in 57.

Compound 58 showed greater binding affinity than 59 due to stronger π–lone pair and π–π interactions with Phe116 (Figure 6C). These binding differences support their observed antimalarial potencies (Manohar, Rajesh, Khan, Tekwani, & Rawat, 2012). Additional docking results for other compounds are shown in Figures S13–S16.

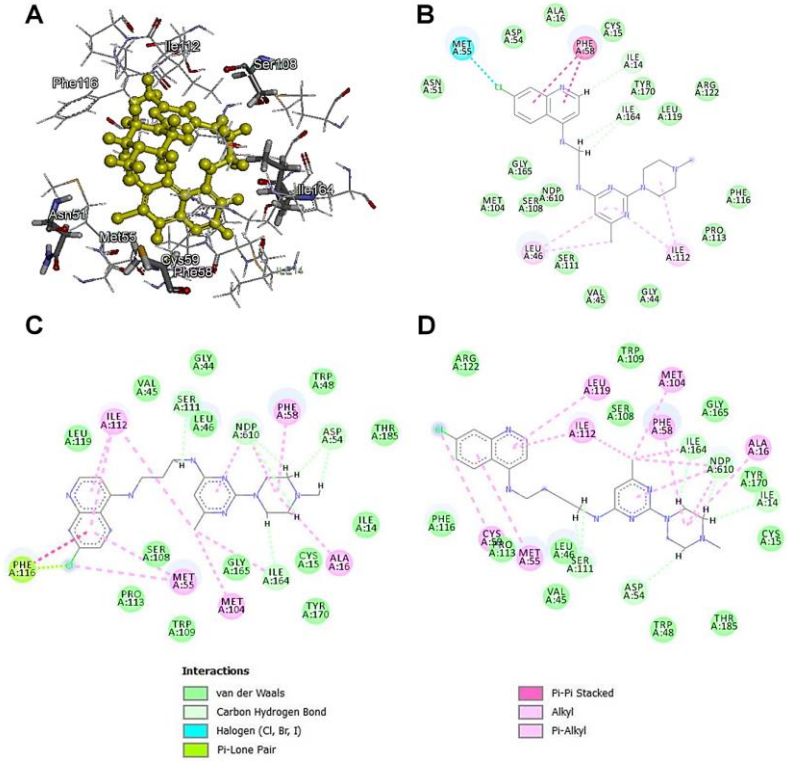

Figure 6. (A, B) Binding interactions (in 3D and 2D) of the docked conformation of the most active compound 57 (pIC_{50} = 8.301), whereas the 2D interactions for its counterpart compounds, 58 (C) and 59 (D), with longer carbon linkers (n = 3 and 4, respectively) were also included for comparison. This visualization was made by using the BIOVIA Discovery Studio. The values of GoldScore fitness for 57, 58 and 59 are 68.00, 73.26, and 71.48, respectively.

3.4 NCI analysis

NCI analysis was performed on compounds 57–59 to characterize key interactions with *Pf*DHFR. The 2D RDG plots (–0.06 to +0.06) and corresponding 3D isosurfaces (Figure 7) reveal dominant van der Waals forces (green regions, –0.02 to +0.02), supporting weak but favorable binding. Compound 57 shows weaker interactions than those observed for compounds 58 and 59 due to less extensive green isosurfaces, correlating with its shorter linker. The interaction strength for the ligand binding can be tracked from the integration of electron density, ρ(r). As shown in Figure S17, the binding strength trend (58 > 59 > 57) is observed, consistent with the docking results above. A significant difference between the shorter linker compound 57 and the longer linker compounds 58-59 is detected in the NCI plots. Additionally, sharp blue RDG peaks (–0.04 to –0.03) in compounds 58–59 indicate H-bonding with the ribose OH of NDP, absent in 57. Overall, the NCI results are consistent with the docking study and further support the role of van der Waals and hydrogen-bond interactions in stabilizing the binding process of *Pf*DHFR.

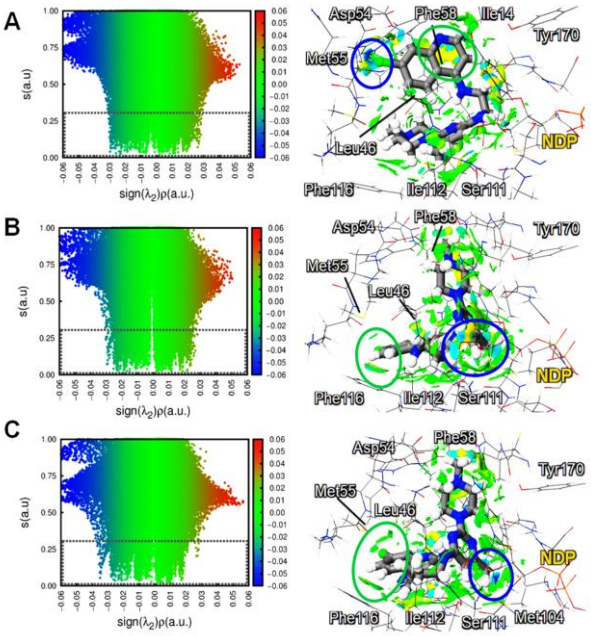

Figure 7. 2D scatters (left) and 3D isosurfaces (right) of the docked conformations of compounds 57 (A), 58 (B) and 59 (C) from NCI analysis. Circles on the 3D NCI plots indicate regions corresponding to important H-bond (blue circles) and van der Waals interactions (green circles) observed for each compound

4. Conclusions

This study employed 3D-QSAR and molecular docking to analyze 162 compounds (4-aminoquinoline-pyrimidine derivatives) as antimalarial agents targeting *Pf*DHFR. CoMFA and CoMSIA models, aligned using

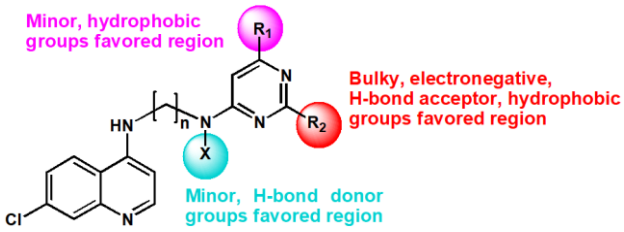

Figure 8. Structural features obtained from this current 3D-QSAR study. Optimal length of the carbon linker is $n = 3$ (> 39% of all studied compounds, Figure 3B).

compound 57, demonstrated good predictive performance (CoMFA: $q^2 = 0.506$, $r^2 = 0.875$, SEE = 0.227; CoMSIA: $q^2 = 0.614$, $r^2 = 0.871$, SEE = 0.230). Key pharmacophoric features were identified from contour maps, recommending small hydrophobic R_1 groups, bulky hydrophobic R_2 groups, and appropriate H-bond donor/acceptor substitutions at R_2 and –NX positions, as shown in Figure 8. Further docking simulations revealed that optimal binding involves interactions with Phe58, Phe116, and the NADPH nicotinamide moiety. Compounds 58 and 59 showed stronger binding due to favorable conformations, while compound 57 lacked key interactions due to a shorter linker. Residues Ile14, Leu46, Met55, Phe58, Ser111, Ile112, Phe116, and Ile164 were identified as crucial for binding stability, as supported by NCI analysis.

Acknowledgements

We thank NECTEC for providing Sybyl-X 2.0 and KURDI, Kasetsart University, for supporting the GOLD license (Grant No. FF(KU) 11.64). J.J. acknowledges support from the University of Phayao, TSRI (Fundamental Fund 2025, Grant No. 5026/2567), and the School of Science, University of Phayao (Grant No. PBTSC67019), including the Unit of Excellence project (FF66-UoE016). W.C. is supported by TSRI and KMITL (Grant Nos. 2564-02-05-021 and FF66-4274282).

References

Balabadra, S., Kotni, M., Manga, V., Allanki, A. D., Prasad, R., & Sijwali, P. S. (2017). Synthesis and evaluation of naphthyl bearing 1,2,3-triazole analogs as antiplasmodial agents, cytotoxicity and docking studies. *Bioorganic and Medicinal Chemistry*, *25*(1), 221–232. doi:10.1016/j.bmc.2016.10.029

Chakraborty, A. (2016). Emerging drug resistance in Plasmodium falciparum: A review of well-characterized drug targets for novel antimalarial chemotherapy. *Asian Pacific Journal of Tropical Disease*, *6*(7), 581–588. doi:10.1016/S2222-1808(16)61090-3

Contreras-García, J., Johnson, E. R., Keinan, S., Chaudret, R., Piquemal, J.-P., Beratan, D. N., & Yang, W. (2011). NCIPLOT: A program for plotting noncovalent interaction regions. *Journal of Chemical Theory and Computation*, *7*(3), 625–632. doi:10.1021/ct100641a

Cramer, R. D., Patterson, D. E., & Bunce, J. D. (1988). Comparative molecular field analysis (CoMFA). 1. Effect of shape on binding of steroids to carrier proteins. *Journal of the American Chemical Society*, *110*(18), 5959–5967. doi:10.1021/ja00226a005

Frisch *et al*. (2009). *Gaussian 09*. Revision D.01, Wallingford, CT, USA: Gaussian Inc.

Gelb, M. H. (2007). Drug discovery for malaria: A very challenging and timely endeavor. *Current Opinion in Chemical Biology*, *11*(4), 440–445. doi:10.1016/j.cbpa.2007.05.038

Jitonnom, J., Meelua, W., Tue-nguen, P., Saparpakorn, P., Hannongbua, S., & Chotpatiwetchkul, W. (2024). 3D-QSAR and molecular docking studies of peptide-hybrids as dengue virus NS2B/NS3 protease inhibitors. *Chemico-Biological Interactions*, *396*, 111040. doi:10.1016/j.cbi.2024.1110 40

Jones, G., Willett, P., Glen, R. C., Leach, A. R., & Taylor R. (1997). Development and validation of a genetic algorithm for flexible docking. *Journal of Molecular Biology*, *267*(3), 727–748. doi:10.1006/jmbi.1996.0897

Klebe, G., Abraham, U., & Mietzner, T. (1994). Molecular similarity indices in a comparative analysis (CoMSIA) of drug molecules to correlate and predict their biological activity. *Journal of Medicinal Chemistry*, *37*(24), 4130–4146. doi:10.1021/jm00050a010

Kumar, D., Khan, S. I., Ponnan, P., & Rawat, D. S. (2014). Triazine–pyrimidine based molecular hybrids: synthesis, docking studies and evaluation of antimalarial activity. *New Journal of Chemistry*, *38*, 5087–5095. doi:10.1039/c4nj00978a

Kumar, D., Khan, S. I., Tekwani, B. L., Ponnan, P., & Rawat, D. S. (2014). Synthesis, antimalarial activity, heme binding and docking studies of 4-aminoquinoline–pyrimidine based molecular hybrids. *RSC Advances*, *4*, 63655–63669. doi:10.1039/C4RA09768H

Kumar, D., Khan, S. I., Tekwani, B. L., Ponnan, P., & Rawat, D. S. (2015). 4-Aminoquinoline-pyrimidine hybrids: Synthesis, antimalarial activity, heme binding and docking studies. *European Journal of Medicinal Chemistry Reports*, *89*, 490–502. doi:10.1016/j.ejmech.2014.10.061

Manohar, S., Khan, S. I., & Rawat, D. S. (2010). Synthesis, antimalarial activity and cytotoxicity of 4-aminoquinoline–triazine conjugates. *Bioorganic & Medicinal Chemistry Letters*, *20*(1), 322–325. doi:10.1016/j.bmcl.2009.10.106

Manohar, S., Rajesh, U. C., Khan, S. I., Tekwani, B. L., & Rawat, D. S. (2012). Novel 4-aminoquinoline-pyrimidine based hybrids with improved in vitro and in vivo antimalarial activity. *ACS Medicinal Chemistry Letters*, *3*(7), 555–559. doi:10.1021/ml3000808

Manohar, S., Tripathi, M., & Rawat, D. S. (2014). 4-aminoquinoline based molecular hybrids as antimalarials: An overview. *Current Topics in Medicinal Chemistry*, *14*, 1706–1733. doi:10.2174/1568026614666140808125728.

Manohar, S., Pavan, V. S., Taylor, D., Kumar, D., Ponnan, P., Wiesner, L., & Rawat, D. S. (2015). Highly active 4-aminoquinoline–pyrimidine based molecular hybrids as potential next generation antimalarial agents. *RSC Advances*, *5*(36), 28171-28186. doi:10.1039/C4RA16032K

Maurya, S. S., Khan, S. I., Bahuguna, A., Kumar, D., & Rawat, D. S. (2017). Synthesis, antimalarial activity, heme binding and docking studies of N-substituted 4-aminoquinoline-pyrimidine molecular hybrids. *European Journal of Medicinal Chemistry Reports*, *129*, 175–185. doi:10.1016/j.ejmech.2017.02.024

Muregi, F. W., & Ishih, A. (2010). Next-generation antimalarial drugs: hybrid molecules as a new strategy in drug design. *Drug Development Research*, *71*, 20–32. doi:10.1002/ddr.20345

Novoa, T., Laplaza, R., Peccati, F., Fuster, F., & Contreras-García, J. (2023). The NCIWEB server: a novel implementation of the noncovalent interactions index for biomolecular systems. *Journal of Chemical Information and Modeling*, *63*(15), 4483–4489. doi:10.1021/acs.jcim.3c00271

Phillips, M. A., Burrows, J. N., Manyando, C., van Huijsduijnen, R. H., Van Voorhis, W. C., & Wells, T.N.C. (2017). Malaria. *Nature Reviews Disease Primers*, *3*, 17050. doi:10.1038/nrdp.2017.50

Reddy, P. L., Khan, S. I., Ponnan, P., Tripathi, M., & Rawat, D. S. (2017). Design, synthesis and evaluation of 4-aminoquinoline-purine hybrids as potential antiplasmodial agents. *European Journal of Medicinal Chemistry*, *126*, 675–686. doi:10.1016/j.ejmech.2016.11.057

Roy, K., Kar, S., & Das, R. N. (2015). Understanding the basics of QSAR for applications in pharmaceutical sciences and risk assessment. In K. Roy, S. Kar & R. N. Das (Eds.), *Understanding the basics of QSAR for applications in pharmaceutical sciences and risk assessment* (pp. 291–317). Boston, MA: Academic Press. doi:10.1016/C2014-0-00286-9

Sharma, M., & Chauhan, P. M. S. (2012). Dihydrofolate reductase as therapeutics target for infectious diseases: opportunities and challenges. *Future Medicinal Chemistry*, *4*(10), 1335−1365. doi:10.4155/fmc.12.68

Tarnchompoo, B., Sirichaiwat, C., Phupong, W., Intaraudom, C., Sirawaraporn, W., Kamchonwongpaisan, S., . . . Yuthavong, Y. (2002). Development of 2,4-diaminopyrimidines as antimalarials based on inhibition of the S108N and C59R+S108N mutants of dihydrofolate reductase from pyrimethamine-resistant Plasmodium falciparum. *Journal of Medicinal Chemistry*, *45*(6), 1244−1252. doi:10.1021/jm010131q

Thakur, A., Khan, S. I., & Rawat, D. S. (2014). Synthesis of piperazine tethered 4-aminoquinoline-pyrimidine hybrids as potent antimalarial agents. *RSC Advances*, *4*(40), 20729–20736. doi:10.1039/C4RA02276A

Tripathi, M., Khan, S., Thakur, A., Ponnan, P., & Rawat, D. (2015). 4-Aminoquinoline-pyrimidine-amino alkanols: Synthesis, *in vitro* antimalarial activity, docking studies and ADME predictions. *New Journal of Chemistry*, *39*, 3474–3483. doi:10.1039/c5nj00094g

Tripathi, M., Khan, S. I., Ponnan, P., Kholiya, R., & Rawat, D.S. (2017). Aminoquinoline-pyrimidine-modified anilines: synthesis, in vitro antiplasmodial activity, cytotoxicity, mechanistic studies and ADME predictions. *ChemistrySelect*, *2*, 9074–9083. doi:10.1002/slct.201701558.*2*

Tue-Ngeun, P., Rakitikul, W., Thinkumrob, N., Hannongbua, S., Meelua, W., & Jitonnom, J. (2024). Binding interactions and in silico ADME prediction of isoconessimine derivatives as potent acetyl cholinesterase inhibitors. *Journal of Molecular Graphics and Modelling*, *129*, 108746. doi:10.1016/j.jmgm.2024.108746

Vanichtanankul, J., Taweechai, S., Yuvaniyama, J., Vilaivan, T., Chitnumsub, P., Kamchonwongpaisan, S., & Yuthavong, Y. (2011). Trypanosomal dihydrofolate reductase reveals natural antifolate resistance. *ACS Chemical Biology*, *6*(9), 905–911. doi:10.1021/cb200124r

Venkatesan, P. (2024). The 2023 WHO World malaria report. *Lancet Microbe*, *5*(3), e214. doi:10.1016/S2666-5247(24)00016-8

Verdonk, M. L., Cole, J. C., Hartshorn, M. J., Murray, C. W., & Taylor, R. D. (2003). Improved protein-ligand docking using GOLD. *Proteins*, *52*(4), 609–623. doi: 10.1002/prot.10465

Wold, S., Ruhe, A., Wold, H., & Dunn, I. W. J. (1984). The collinearity problem in linear regression. The partial least squares (PLS) approach to generalized inverses. *SIAM Journal on Scientific Computing*, *5*(3), 735–743. doi:10.1137/0905052